Stably Supported Rotations of a Planar Polygon with Two Frictionless Contacts *

Tamara Abell
Robotics Institute
Carnegie Mellon University
Pittsburgh, PA 15213-3891

Michael Erdmann
Robotics Institute
Carnegie Mellon University
Pittsburgh, PA 15213-3891

Abstract

In this paper, we explore the use of stable support *in robotic manipulation. Stable support describes any contact configuration which balances a known applied force and is stable with respect to small perturbations in the handled object's pose. Specifically, we address the problem of manipulating a planar polygonal object in a fixed gravitational field, stably supported by two frictionless contacts. Representing each contact configuration as a* force focus *point defined by the intersection of the lines of action of the contact forces, we derive geometric regions of permissible force focus points for contacts on each pair of polygon edges. Each permissible force focus point maps to a unique configuration of the object and contacts in stable equilibrium. In turn, paths in the space of permissible force focus points map to real space motions of the contact points which induce quasi-static rotations of the object. We also present two graph search based strategies for planning hand-offs between pairs of contacts, thus enabling larger rotations than can be executed by a single contact pair. Finally, we describe an implementation of one of these planners.*

1. Introduction

A key subtask in robotic manipulation is to position and orient an object while maintaining contact with the robot's hand. One approach to this problem is to fix the object relative to the hand by grasping it. Much research on grasping has focused on force closure grasps, which can resist any applied force and torque with an appropriate choice of contact forces. Once grasped, the object is manipulated by moving the entire hand. Other work has addressed shifting the points of contact while maintaining force closure, thus reconfiguring the object relative to the hand.

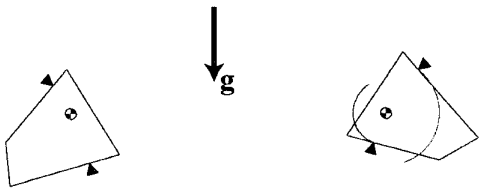

Figure 1: Stably supported rotation under gravity.

These strategies are powerful because the grasp can be maintained in the face of arbitrary applied forces. Unfortunately, robot and task constraints can combine to make force closure impossible. For example, limited finger number and dexterity, assembly constraints and untouchable object surfaces can all affect the existence of force closure grasps. Also, some tasks, such as transport, re-orienting and passing an object between robots, may not require the broad resistance to external forces provided by force closure.

In this context, we are motivated to explore the use of *stable support* in place of grasping for robotic manipulation. Stable support describes a contact configuration which balances a known applied force and is stable with respect to small perturbations in the object's pose. Figure 1 depicts two moving fingers rotating a polygonal object in a gravitational field. At each instant, the object is stably supported by the finger contacts. In general, stable support requires fewer contacts than a force closure grasp. Thus, manipulation strategies using stable support may succeed where grasps do not exist.

This paper addresses the specific task of manipulating a planar polygonal object in a fixed gravitational field, stably supported by two frictionless contacts. Markenscoff et. al. [10] have shown that at least four such contacts are necessary for force closure in the plane. Therefore, this problem is a suitable context for exploring stable support. First, we derive geometric regions of permissible *force focus* points for contacts on each pair of polygon edges. A force focus [3] is defined as the intersection of the lines

* Support for this research was provided in part by Carnegie Mellon University, in part by a National Science Foundation fellowship, in part by a NASA-JPL fellowship, and in part by the National Science Foundation through the following grants: NSF Research Initiation Award IRI-9010686 and NSF Presidential Young Investigator award IRI-9157643. Any opinions, findings, conclusions or recommendations expressed in this document are those of the authors and do not necessarily reflect the views of the National Science Foundation or NASA-JPL.

0-8186-7108-4/95 $4.00

of action of the contact reaction forces. Each permissible force focus point maps to a unique configuration of the object and contacts in stable equilibrium. In turn, paths in the space of permissible force focus points map to real space motions of the contact points which induce quasi-static rotations of the object. Next we present two graph search based strategies for planning hand-offs between pairs of contacts. These hand-offs enable larger rotations than can be executed by a single contact pair. Finally, we describe an implementation of one of these planners.

1.1. Related work

In the area of grasping, Mishra, et. al. [12] derive upper bounds on the number of contacts necessary for force closure as a function of the dimensionality of the force/torque space. Nguyen [14] describes algorithms for constructing force closure grasps of polygons and polyhedra. Using a representation analogous to the force focus, Markenscoff and Papadimitriou [11] address the problem of finding optimal force closure grasps. Park and Starr [15] develop a simple algorithm for constructing three-fingered force closure grasps of planar polygons. Salisbury and Craig [17] address the design of robot hands for manipulating objects under force closure. Both Montana [13] and Trinkle [18] propose methods for evaluating the stability of force closure grasps. Fearing [6] defines finger-level requirements for stable grasps in the plane and explores the use of a third finger to induce rotations. Howard and Kumar [7] analyze the stability of planar non-force closure grasps, including grasps of convex polygons by point contacts.

In other related work, Trinkle, Farahat, and Stiller [19, 20] develop a general framework for characterizing first and second order configuration space (C-space [9]) stability regions for polyhedra in frictionless contact. Our work addresses the two dimensional version of this problem in a different planning space where the stable regions have very simple geometries. Brock [3] uses the term force focus in the context of his analysis of controlling slip in response to an applied force. Yoshikawa et. al. [21] analyze slipping motions in the context of three fingered grasps with friction. Kao and Cutkosky [8] also investigate manipulation with sliding contacts. Rus [16] derives a method for rotating polygons within a three fingered equilibrium grasp. Our work is closely related to this, employing a gravitational applied force in place of a third finger. Balorda [2] addresses the problem of orienting a part by pushing in two point contact; his use of two contacts to constrain the pose of the object is similar to that presented here. Brost [4] uses a C-space representation and energy arguments to compute the relative resting poses of two polygons in contact.

2. Problem statement

Let $\mathcal{B}$ be a convex polygonal body in the plane, contacted by two fingers at two points on its perimeter. A gravity force $\mathbf{g}$ acts on $\mathcal{B}$. The pose of $\mathcal{B}$ in the world frame W and the locations of the contacts relative to $\mathcal{B}$ denote a *contact configuration*. We want to plan rotations of $\mathcal{B}$ in the space of *stably supported* contact configurations. The components of this task are:

- Characterize all contact configurations in which $\mathcal{B}$ is stably supported.
- Plan contact motions which induce quasi-static rotations of $\mathcal{B}$ while maintaining stable support.
- Plan stably supported hand-offs between finger pairs.

Our solution assumes exact knowledge of the geometry, mass properties and initial pose of $\mathcal{B}$. Contacts between the fingers and $\mathcal{B}$ are modelled as frictionless point contacts. We also assume that the contact points can be precisely positioned relative to the world frame, without addressing finger motion planning and contact feasibility. Finger motions are assumed to be sufficiently slow to justify a quasi-static model.

3. Characterizing stable support

In this section, we characterize the space of stably supported contact configurations with contacts on edges e_i and e_k of $\mathcal{B}$. To this end, it is useful to view the contact configurations in two distinct frames, a world frame W and the body frame B. Figure 2 shows a contact configuration in frame W. For convenience, we choose W so that $\mathbf{g}$ acts along its $-y$-axis. The points of contact are denoted by $\mathbf{p}_i$ and $\mathbf{p}_k$. Their difference, $\mathbf{p}_\Delta = \mathbf{p}_k - \mathbf{p}_i$, is specified by length p_Δ and angle ξ measured relative to W. The pose of body frame B in frame W is given by $\mathbf{b}$ and θ.

$\mathbf{n}_i$ and $\mathbf{n}_k$ denote the inward unit normals to edges e_i and e_k of $\mathcal{B}$. These vectors make angles α_i and α_k with the x-axis of B. We will show that configurations with two contacts on one edge or contacts on parallel edges (whenever $\mathbf{n}_i \times \mathbf{n}_k = 0$) are at best marginally stable; thus, our analysis assumes that $\mathbf{n}_i$ and $\mathbf{n}_k$ are linearly independent. We label the edges such that $\mathbf{n}_i \times \mathbf{n}_k > 0$. $\mathbf{t}_i$ and $\mathbf{t}_k$ denote the unit tangents, chosen so that $\mathbf{t}_i \cdot \mathbf{n}_k \geq 0$ and $\mathbf{t}_k \cdot \mathbf{n}_i \geq 0$. Virtual vertex $\mathbf{V}$ locates the intersection of the edge lines; for adjacent edges, $\mathbf{V}$ is a vertex of $\mathcal{B}$. $\mathbf{V}$ is specified by length l and angle γ measured in frame B. Note that α_i, α_k, γ and l are fixed by the geometry of $\mathcal{B}$. $\mathbf{c}_f$ denotes the force focus at the intersection of the lines of action of the contact forces. Since the contacts are zero friction, these forces are $f_i\mathbf{n}_i$ and $f_k\mathbf{n}_k$, where $f_i, f_k \geq 0$.

Observe that the forces acting on $\mathcal{B}$ are translationally invariant, depending only on θ and the locations of the contacts relative to $\mathcal{B}$. These contact locations are given uniquely by projecting the force focus onto the contact edges in the body frame. The mapping between $\mathbf{c}_f^B$ and the contact locations is invertible, since the normals are linearly independent. Thus, the criteria for stable support, specifically geometric contact, force balance and stability, depend only on the *local contact configuration* given by $(\mathbf{c}_f^B, \theta)$. We will show that the force focus alone is sufficient to characterize all *equilibrium* configurations,

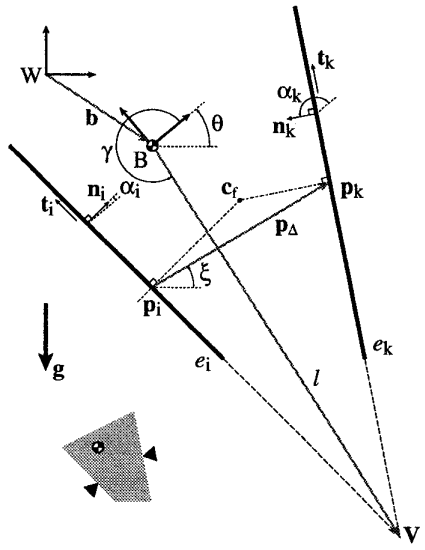

Figure 2: A contact configuration in world frame W, with gravity along the $-y$-axis. $\mathbf{b}$ and θ locate body frame B in frame W. The edge normal angles α_i and α_k are measured in frame B, as are γ and l, which locate the virtual vertex $\mathbf{V}$. Force focus $\mathbf{c}_f$ marks the intersection of the lines of force through contacts $\mathbf{p}_i$ and $\mathbf{p}_k$. Vector $\mathbf{p}_\Delta$ connects the contacts and lies at angle ξ in frame W.

and thus all stably supported ones, with contacts on edges e_i and e_k.

3.1. Mapping force focus to equilibrium orientation

Consider the set of local contact configurations with a fixed force focus $\mathbf{c}_f^B$ in frame B. Figure 3 depicts one such configuration. Observe that in the body frame, the applied force $\mathbf{g}^B$ varies with θ:

$$\mathbf{g}^B = -mg \begin{bmatrix} \sin(\theta) \\ \cos(\theta) \end{bmatrix}, \tag{1}$$

with g the gravitational constant and m the mass of $\mathcal{B}$. Clearly, any equilibrium orientation ψ corresponds to a vector $\mathbf{g}^B$ which can be balanced by the contact forces. We can write the force balance equations with the contact forces applied at $\mathbf{c}_f^B$, the intersection of their lines of action:

$$f_i\mathbf{n}_i^B + f_k\mathbf{n}_k^B = -\mathbf{g}^B, \tag{2}$$

$$(f_i\mathbf{n}_i^B + f_k\mathbf{n}_k^B) \times -\mathbf{c}_f^B = 0, \tag{3}$$

where $f_i, f_k \geq 0$. Together these imply:

$$\mathbf{g}^B \times \mathbf{c}_f^B = 0. \tag{4}$$

By Equation 4, the line of action of the applied force must pass through the force focus at equilibrium. Viewed in

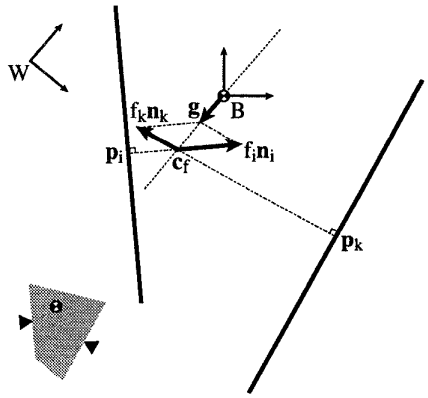

Figure 3: An equilibrium contact configuration in frame B. Contact forces $f_i\mathbf{n}_i$ and $f_k\mathbf{n}_k$, acting at $\mathbf{c}_f$, balance $\mathbf{g}$.

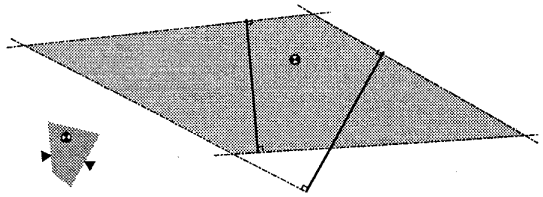

Figure 4: Contact constraints. Force foci of feasible geometric contacts lie in the shaded region.

frame B where the force focus is fixed, this means that $\mathbf{c}_f^B$ determines the line of action of $\mathbf{g}^B$. Further, Equation 2 constrains $\mathbf{g}^B$ to the negative span of the contact normals. Since $\mathbf{n}_i^B$ and $\mathbf{n}_k^B$ are linearly independent, at most one vector $\mathbf{g}^B$ satisfies both equations. Thus, for contacts on e_i and e_k, each $\mathbf{c}_f^B$ maps to at most one equilibrium orientation ψ of $\mathcal{B}$. We conclude that $\mathbf{c}_f^B$ alone is sufficient to characterize all equilibrium configurations $(\mathbf{c}_f^B, \psi)$.

3.2. Constraints on force focus

Force foci represent equilibrium contact configurations simply, as points in the body frame. Not all these points correspond to feasible, stable equilibria. By mapping the constraints for geometric contact, force balance and stability onto the plane, we can delimit regions of *permissible* force foci, corresponding to local contact configurations exhibiting stable support.

To represent a feasible contact geometry, the force focus must project onto both edges. Thus, $\mathbf{c}_f$ must lie in a region bounded by normal lines through the endpoints of each edge. Figure 4 shows this *contact constraint* region for edges e_i and e_k of $\mathcal{B}$.

Next we derive the *equilibrium constraint*. Recall that at equilibrium, $\mathbf{c}_f^B$ lies on the line of action of $\mathbf{g}^B$, which in turn must lie in the negative span of $\mathbf{n}_i^B$ and $\mathbf{n}_k^B$. Thus, normal lines through the center of mass bound the

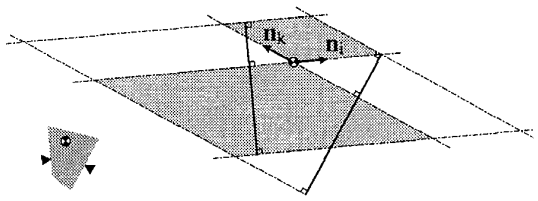

Figure 5: Equilibrium and contact constraints. Shaded force foci map to feasible, equilibrium contact.

equilibrium constraint, with $\mathbf{c}_f^B$ in either the positive or the negative span. Figure 5 shows the intersection of the equilibrium and contact constraints.

In order to gain geometric insight and treat forces and torques consistently, we examine the *stability constraints* on $\mathbf{c}_f^B$ in the configuration space (C-space) of $\mathcal{B}$. The pose of $\mathcal{B}$ in C-space coordinates is given by

$$\mathbf{b}_c = \left[b_x^W, b_y^W, \rho\theta\right]^\top, \tag{5}$$

with ρ the radius of gyration of $\mathcal{B}$. Suppose $\mathcal{B}$ is in contact along a given edge with a point fixed in the world frame. As $\mathcal{B}$ moves while maintaining this contact, $\mathbf{b}_c$ travels on a two dimensional surface in C-space. This surface is the *constraint surface* representing the motion constraints imposed on $\mathcal{B}$ by the contact.

Contacts $\mathbf{p}_i^W$ and $\mathbf{p}_k^W$ on edges e_i and e_k give rise to two C-space constraint surfaces. Their intersection is a curve of configurations of $\mathcal{B}$ in two point contact, called the *constraint curve*. The outward normals to the constraint surfaces are

$$\mathbf{n}_{ic} = \begin{bmatrix} n_{ix}^W \\ n_{iy}^W \\ \frac{n_{iq}}{\rho} \end{bmatrix}, \qquad \mathbf{n}_{kc} = \begin{bmatrix} n_{kx}^W \\ n_{ky}^W \\ \frac{n_{kq}}{\rho} \end{bmatrix}, \tag{6}$$

where $n_{iq} = \mathbf{n}_i^B \times \mathbf{p}_i^B$ and $n_{kq} = \mathbf{n}_k^B \times \mathbf{p}_k^B$. Note that $\mathbf{n}_{ic}$ and $\mathbf{n}_{kc}$ are not unit normals. Erdmann [5] has shown that the force and torque equilibrium equations can be written

$$f_i\mathbf{n}_{ic} + f_k\mathbf{n}_{kc} = -\mathbf{g}_c, \tag{7}$$

where $\mathbf{g}_c = [0, -mg, 0]^\top$ is the applied force and torque and $f_i, f_k \geq 0$ are the contact force magnitudes. Note that this equation also describes the balance of forces on a particle in frictionless contact with the two constraint surfaces. This view is useful in visualizing stability in C-space coordinates.

At stable equilibrium, small perturbations in the body pose result in restoring forces which return $\mathbf{b}_c$ to equilibrium. Equivalently, $\mathbf{b}_c$ must be a potential energy minimum of $\mathcal{B}$. We can visualize this as the particle lying at a minimum in y on the intersection of the constraint surfaces. Functionally, this means that any valid motion (one allowed by the contact constraints) opposes $\mathbf{g}_c$.

Let $\mathbf{v}$ specify a motion of $\mathcal{B}$ in C-space. For generic (i.e., non-vertex) contacts, each constraint surface limits $\mathbf{v}$ to a half-space bounded by its tangent plane at $\mathbf{b}_c$. The intersection of these two half-spaces is the set of valid motions $\mathbf{v}$. Formally, this set is

$$\left\{\mathbf{v} \in \mathcal{R}^3 \middle| \mathbf{v} \cdot \mathbf{n}_{ic} \geq 0 \text{ and } \mathbf{v} \cdot \mathbf{n}_{kc} \geq 0\right\}. \tag{8}$$

The force focus $\mathbf{c}_f^B$ maps to a stable equilibrium configuration if for all valid $\mathbf{v}$, either $\mathbf{v} \cdot \mathbf{g}_c < 0$ or both $\mathbf{v} \cdot \mathbf{g}_c = 0$ and second order features of the constraint surfaces cause a potential energy minimum. These stability conditions are termed *first order* and *second order* respectively [19, 20]. Specific second order stability criteria will be developed as needed.

Observe that the C-space normals $\mathbf{n}_{ic}$ and $\mathbf{n}_{kc}$ are linearly independent, since they derive from the contact normals $\mathbf{n}_i^W$ and $\mathbf{n}_k^W$. Together with their mutual tangent $\mathbf{t}_c = \mathbf{n}_{ic} \times \mathbf{n}_{kc}$, they form a basis of the C-space of $\mathcal{B}$. Thus, $\mathbf{v}$ can be divided into a normal component $\mathbf{v}_n$ in the plane of $\mathbf{n}_{ic}$ and $\mathbf{n}_{kc}$ and a tangential component $\mathbf{v}_t$ along $\mathbf{t}_c$. Let us first examine the stability constraints imposed by nonzero normal motions $\mathbf{v}_n$.

To assess stability under normal motions, we must examine the value of $\mathbf{v} \cdot \mathbf{g}_c$. Note that at equilibrium, the tangential component of $\mathbf{v}$ is normal to the plane of the C-space normals containing $\mathbf{g}_c$. Thus, substituting for $\mathbf{g}_c$ with Equation 7, we can write the stability expression as

$$\mathbf{v} \cdot \mathbf{g}_c = -f_i(\mathbf{v}_n \cdot \mathbf{n}_{ic}) - f_k(\mathbf{v}_n \cdot \mathbf{n}_{kc}) \leq 0. \tag{9}$$

This inequality holds since $\mathbf{v}_n \cdot \mathbf{n}_{ic} \geq 0$ and $\mathbf{v}_n \cdot \mathbf{n}_{kc} \geq 0$ for all valid motions. Hence, an equilibrium configuration is first order stable under normal motions except when the inequality is zero, that is, when $\mathbf{v}_n$ is orthogonal to $\mathbf{g}_c$.

Observe that when the stability expression in Equation 9 equals zero, each component of the sum is also zero. For nonzero $\mathbf{v}_n$, at most one of the dot products can be zero, since the C-space normals are linearly independent and $\mathbf{v}_n$ lies in their common plane. Similarly, at least one of f_i and f_k is nonzero. Hence, the stability expression is zero only if $f_i = (\mathbf{v}_n \cdot \mathbf{n}_{kc}) = 0$ or $f_k = (\mathbf{v}_n \cdot \mathbf{n}_{ic}) = 0$. In particular, gravity must lie along one of the negated contact normals, either $\mathbf{g}_c = -f_k\mathbf{n}_{kc}$ or $\mathbf{g}_c = -f_k\mathbf{n}_{kc}$. At equilibrium, this implies that the force focus lies on a boundary of the equilibrium constraint (see Figure 5). We will show by example that force foci on these boundaries map to unstable equilibria.

Consider a feasible contact configuration with $\mathbf{c}_f^B$ on the equilibrium constraint boundary derived from $\mathbf{n}_i^B$, such that $f_k = 0$. In C-space coordinates, we have $\mathbf{g}_c = -f_i\mathbf{n}_{ic} = [0, -mg, 0]^\top$ and $\mathbf{n}_{ic} = [0, 1, 0]^\top$. Figure 6 illustrates this case. Let $\mathbf{v}_0$ be the C-space velocity corresponding to pure translation along $\mathbf{t}_i^W$,

$$\mathbf{v}_0 = v_0\,[1, 0, 0]^\top. \tag{10}$$

Since $\mathbf{t}_i \cdot \mathbf{n}_k \geq 0$, this motion is valid. Also, the stability expression $\mathbf{v}_0 \cdot \mathbf{g}$ is zero. Observe that motion along $\mathbf{v}_0$ maintains contact along the edge e_i and that the corresponding trajectory on the C-space constraint

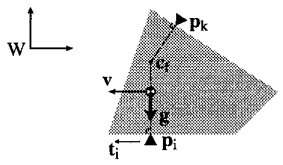

Figure 6: An unstable contact configuration corresponding to $\mathbf{c}_f^B$ on the boundary of the equilibrium constraint. Vector $\mathbf{v}$ is a pure translation in the direction of $\mathbf{t}_i$.

surface is linear with constant y. Thus, a minimum in y does not exist. After an initial translation, the torque due the maintained contact $\mathbf{p}_i^W$ will rotate the body further from the equilibrium configuration. Hence, the contact configuration is *unstable*. A similar argument applies when $\mathbf{c}_f^B$ lies on the $\mathbf{n}_k^B$ equilibrium constraint boundary. We conclude that force foci on the interior of the equilibrium constraint map to first order stable contacts, while those on the boundary map to unstable equilibria.

Similar reasoning shows that configurations with linearly dependent contact normals are at best marginally stable. When $\mathbf{n}_i$ and $\mathbf{n}_k$ are linearly dependent, there exists a valid translational motion $\mathbf{v}_0 = v_0\mathbf{t}_i = v_0\mathbf{t}_k$ orthogonal to both C-space normals. At equilibrium, $\mathbf{g}^W$ is parallel to $\mathbf{n}_i^W$ and $\mathbf{n}_k^W$, thus $\mathbf{v}_0 \cdot \mathbf{g}^W = 0$. By the above argument, we know that motion along $\mathbf{v}_0$ is linear and has no minimum in y. Depending on the contact configuration, a motion along $\mathbf{v}_0$ may lead either to instability or to a new equilibrium pose. In the later case, the contact configuration is labeled *marginally stable*.

Having derived the stability constraints imposed by normal motions, we return to consider purely tangential motions $\mathbf{v} = \mathbf{v}_t$. Recall that at equilibrium, $\mathbf{v}_t$ is orthogonal to $\mathbf{g}_c$. The stability expression becomes

$$\mathbf{v}_t \cdot \mathbf{g}_c = 0, \tag{11}$$

forcing us to evaluate second order stability.

Observe that the motion $\mathbf{v}_t$ maintains both contacts; it displaces $\mathbf{b}_c$ along the constraint curve at the intersection of the C-space constraint surfaces. We can write this curve as a function of orientation, $\mathbf{b}_c(\theta)$.[1] Recall that ψ denotes the particular equilibrium orientation for $\mathbf{c}_f^B$. Hence, for stability, $\mathbf{b}_c(\theta)$ evaluated at ψ must be a minimum in y of the constraint curve.

To transform conditions for a minimum of $\mathbf{b}_c(\theta)|_\psi$ into constraints on the force foci, we must relate $\mathbf{c}_f^B$ and ψ. We can write $\mathbf{c}_f^B$ in terms of ψ as follows:

$$\mathbf{c}_f^B = -r \begin{bmatrix} \sin(\psi) \\ \cos(\psi) \end{bmatrix}, \tag{12}$$

where r may be positive or negative. This parameterization holds only where ψ exists, specifically, for $\mathbf{c}_f^B$ within the

[1] $\mathbf{b}_c(\theta)$ projects a conchoid of a circle onto the x-y plane.

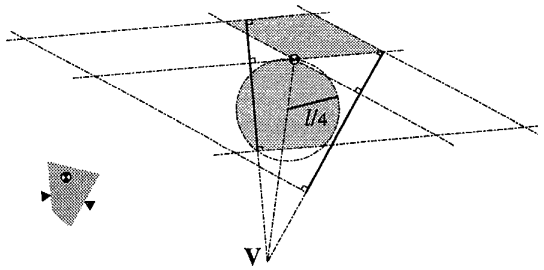

Figure 7: The shaded regions depict the intersection of the contact, equilibrium and stability constraints.

equilibrium constraint boundaries. We may state this limit as

$$\psi \in [\pi/2 - \alpha_k, \pi/2 - \alpha_i]. \tag{13}$$

The span of this range is less than π, since $\mathbf{n}_i \times \mathbf{n}_k > 0$. At most one of ψ and $\psi + \pi$ lies in this range. Thus, the parameterization of $\mathbf{c}_f^B$ is well-defined.

Given Equation 12, we can write $\mathbf{b}_c(\theta)$ as a parameterized function of r and ψ. See Abell and Erdmann [1] for this derivation. Evaluating the second derivative of the y element at ψ, we get

$$\frac{d^2}{d\theta^2} b_{cy}(\theta)\bigg|_\psi = -l\sin(\psi + \gamma) - 2r. \tag{14}$$

For a minimum, the second derivative must be greater than zero. Therefore, the tangential stability constraint is

$$r < \frac{-l\sin(\psi + \gamma)}{2}. \tag{15}$$

We can also write this constraint as

$$r < \frac{1}{2}\mathbf{V}^B \cdot \hat{\mathbf{g}}^B, \tag{16}$$

where $\hat{\mathbf{g}}^B = [-\sin(\psi), -\cos(\psi)]^\top$ is the gravity direction at equilibrium in frame B. The constraint boundary lies on a circle centered at $\frac{1}{4}\mathbf{V}^B$ with radius $l/4$. When the center of mass of $\mathcal{B}$ is contained within its perimeter, vertex $\mathbf{V}^B$ lies in the negative span of the edge tangents. We know also that $\hat{\mathbf{g}}^B$ lies in the negative span of $\mathbf{n}_i$ and $\mathbf{n}_k$. Thus, $\mathbf{V}^B \cdot \hat{\mathbf{g}}^B \geq 0$ on the equilibrium range of ψ (Equation 13). In this case, Equation 16 places a positive upper bound on the values of r. Note also that the stability of $\mathbf{c}_f^B$ is undetermined on the constraint boundary. Figure 7 shows the intersection of the contact, equilibrium, and stability constraints.

Above we have derived the linear and quadratic constraints $\mathbf{c}_f^B$ must satisfy to represent a stable support configuration for contacts on edges e_i and e_k. Their intersection is a set of planar regions of permissible force focus points. Observe that the contact and equilibrium constraints are bounded by lines parallel to the edge normals. Thus, their intersection consists of at most two

parallelogram-shaped regions. Intersecting one of the parallelograms (corresponding to positive r) with the tangential stability curve (the boundary of Equation 16) yields the permissible regions for $\mathbf{c}_f^B$. Careful examination of Equation 16 shows that for convex bodies, these regions are convex. This algorithm, iterated over all edge pairs, generates every stable support configuration for a convex polygonal body.

4. Manipulation in stable support

In this section, we show how paths within the permissible force focus regions are used to plan stably supported rotations of $\mathcal{B}$. Let us define contact positions in the world frame by

$$\mathbf{p}_i^W = \mathbf{b}^W + R_\psi[d_i + (\mathbf{c}_f^B \cdot \mathbf{t}_i^B)\mathbf{t}_i^B],$$
$$\mathbf{p}_k^W = \mathbf{b}^W + R_\psi[d_k + (\mathbf{c}_f^B \cdot \mathbf{t}_k^B)\mathbf{t}_k^B], \qquad (17)$$

where d_i and d_k are the distances from each edge to the center of mass of $\mathcal{B}$. Matrix R_ψ encodes rotation by ψ. Observe that $\mathbf{p}_i^W$ and $\mathbf{p}_k^W$ are continuous functions of the variables b_x^W, b_y^W, ψ and r. As a consequence, a connected path within a permissible force focus region maps to continuous motions of the contacts $\mathbf{p}_i^W$ and $\mathbf{p}_k^W$.

These contact motions induce continuous deformations of the C-space constraint surfaces and thus a continuous motion of the energy minimum at their intersection. So long as $\mathbf{c}_f^B$ is permissible, a minimum exists. We assume that the contacts move sufficiently slowly to justify a quasi-static model of motion. Therefore, we expect the pose of $\mathcal{B}$ to track the energy minimum as $\mathbf{c}_f^B$ moves along a permissible path.

Recall that the permissible regions of convex polygonal bodies are convex. Thus, the linear path between any two force foci in a permissible region is also contained within the region. Figure 1 illustrates a rotation of $\mathcal{B}$ planned using such a path. For contacts on edges e_i and e_k, the equilibrium and stability constraints limit stably supportable orientations ψ to the open interval $(\pi/2 - \alpha_k, \pi/2 - \alpha_i)$, a span of less than π. Contact constraints may narrow it further. Hence, the next section explores hand-off strategies for achieving larger rotations.

4.1. Hand-offs between contact pairs

We define a hand-off to be an instantaneous transition from a particular stable support configuration with contacts on edges e_i and e_k to another with contact edges e_l and e_m. To plan such hand-offs, we must identify the possible transitions from $\mathbf{c}_{fik}$ in one permissible region to $\mathbf{c}_{flm}$ in another. Figure 8 depicts a rotation sequence with a single hand-off shown in the center frame. Observe that $\mathbf{c}_{fik}$ and $\mathbf{c}_{flm}$ must both map to a single stably supported orientation ψ of $\mathcal{B}$. Thus, ψ_{ik} must equal ψ_{lm}.

Using this observation, we can construct a planning graph, shown in Figure 9. Each graph node encodes both the permissible force focus regions for an edge pair e_i and

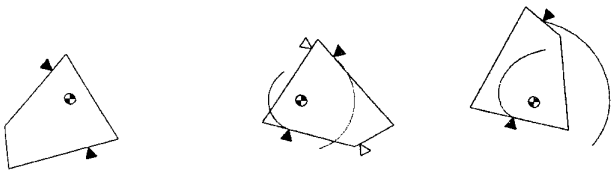

Figure 8: Execution of the rotation plan. Open triangles depict the receiving fingers during a hand-off.

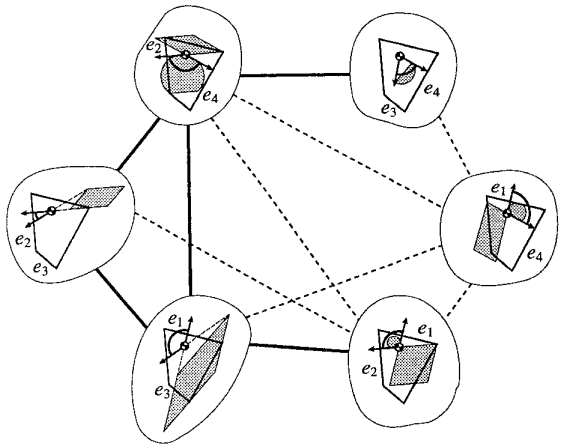

Figure 9: A planning graph. Each node shows the permissible regions for contacts on the labeled edge pair. Angles encode the possible equilibrium orientations as open intervals of supportable applied forces. Solid lines connect nodes whose angle intervals overlap, while dashed lines connect nodes whose open intervals share only a common boundary.

e_k and the interval spanned by ψ within these regions. When two regions are present, at least one spans the entire angle interval, meaning that a force focus trajectory within this region can reach any orientation in the interval. Solid lines connect pairs of nodes when their angle intervals overlap.

To construct a rotation plan, we search the graph for a path from a node containing the initial orientation to a node containing the desired one. Since connectivity is determined only by ψ interval overlap, if any plan exists then there is also a plan with either purely clockwise or purely counterclockwise rotations. For each transition, we chose an angle ψ from the intersection of the angle intervals of adjacent nodes and select $\mathbf{c}_{fik}$ and $\mathbf{c}_{flm}$ from the corresponding permissible regions along this line of action. The initial and final contact configurations are chosen similarly. Within each region, a linear path connecting the receiving and releasing force focus points completes the plan.

Not that for some object geometries, $\mathcal{B}$ cannot be stably supported at all orientations by only two contacts.

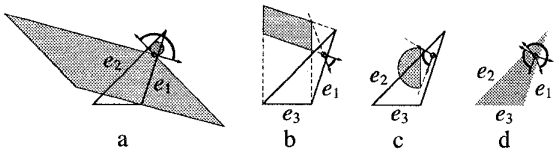

Figure 10: A triangle with unsupportable orientations. Arcs in diagrams a, b and c delimit the applied force directions (equivalently, object orientations) with stable supporting contacts on the labeled edges. Diagram d shows the union of these angle ranges. Gaps correspond to unsupportable orientations.

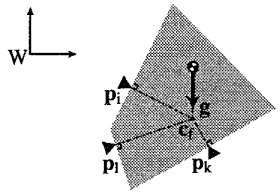

Figure 11: A three fingered hand-off at the instant of transition from contact at $\mathbf{p}_i$ to contact at $\mathbf{p}_l$.

When this happens, we cannot plan rotations passing through or terminating in the unsupportable orientations. In particular, no path exists in the planning graph. Figure 10 depicts a triangular object with two ranges of unsupportable orientations. Diagrams a, b and c depict permissible regions arising from contact on the given edge pairs and the ranges of applied force directions which can be stably supported by $\mathbf{c}_f^{\mathcal{B}}$ in these regions. Diagram d shows the union of these angle ranges, representing all values of ψ for which stable support configurations exist. Gaps correspond to unsupportable orientations of $\mathcal{B}$.

4.2. Hand-offs maintaining one contact

Sometimes it is useful to plan rotations which transfer only one contact at a time. For example, we may want to replace a contact on edge e_i with one on e_l while maintaining contact with e_k. Figure 11 illustrates this case. Such plans are suited to three fingered robots and to situations where assembly constraints or finger dexterity preclude using four fingers to execute a hand-off. We address this planning problem with a graph search based strategy as in Section 4.1. However, here the transition criteria are more stringent. The conditions for transitioning from $\mathbf{c}_{fik}$ in one permissible region to $\mathbf{c}_{fkl}$ in another are:

- The two regions derive from a common edge e_k.
- $\psi_{ik} = \psi_{kl}$; the angle intervals of the regions overlap.
- $\mathbf{c}_{fik}$ and $\mathbf{c}_{fkl}$ project to the same point $\mathbf{p}_k$ on e_k.

To facilitate planning, we will rephrase the last condition in terms of geometric intersections of permissible regions. Observe that both $\mathbf{c}_{fik}$ and $\mathbf{c}_{fkl}$ must lie on the intersection of the line of action of $\mathbf{g}^{\mathcal{B}}$ and on the line normal to e_k through $\mathbf{p}_k$. These lines coincide only for force foci on the unstable equilibrium constraint boundaries. Hence, the intersection of the normal line and the line of force is unique. $\mathbf{c}_{fik}$ and $\mathbf{c}_{fkl}$ denote a single transition force focus point, $\mathbf{c}_{fk}$, which lies in the intersection of the two permissible regions.

Observe that in general, $\mathbf{c}_{fk}$ has two parameterizations,

$$\mathbf{c}_{fk} = -r \begin{bmatrix} \sin(\phi) \\ \cos(\phi) \end{bmatrix}, \quad \mathbf{c}_{fk} = r \begin{bmatrix} \sin(\phi + \pi) \\ \cos(\phi + \pi) \end{bmatrix}, \quad (18)$$

corresponding to $\psi = \phi$ and $\psi = \phi + \pi$ respectively. Exactly one parameterization holds over each permissible region, due to the equilibrium constraints on ψ (see Equation 13). By the hand-off criteria above, we know that ψ_{ik} must equal ψ_{kl}. Thus, $\mathbf{c}_{fk}$ must have identical parameterizations in both permissible regions. This is insured by the angle interval overlap condition.

We can now restate the hand-off criteria as follows:

- The two regions derive from a common edge e_k.
- $\psi_{ik} = \psi_{kl}$; the angle intervals of the regions overlap.
- $\mathbf{c}_{fk}$ lies in the planar intersection of the two regions.

Given these we can build a planning graph. Each node in this graph represents a single permissible region. Arcs connecting the nodes derive directly from the transition criteria. Plans are generated as in the previous algorithm, except that transition force focus points $\mathbf{c}_{fk}$ are chosen from the intersection of adjacent permissible regions. Since connectedness is determined by region overlap versus simply angle overlap, it may be necessary to combine clockwise and counterclockwise rotations to reach a desired orientation. Given that the hand-off criteria are more restrictive, we expect this algorithm fail to find a rotation plan for objects where the first strategy succeeds.

5. Implementation

We have implemented a rotation planner using the four finger hand-off strategy. Given a convex polygonal object $\mathcal{B}$, this planner constructs the permissible regions for each non-parallel edge pair based on a set of simple primitives for intersecting lines and arcs. In this implementation, we have included the unstable boundaries of the equilibrium constraints as part of each permissible region. Inclusion of these boundaries significantly increases the connectivity of the planning graph, as shown by the dashed lines in Figure 9. We are interested in whether these unstable configurations are usable in transition.

From the permissible regions, we build a directed planning graph as outlined in Section 4.1. Given initial and goal orientations for $\mathcal{B}$, the planner searches the graph for all paths connecting these orientations in the specified direction (clockwise or counterclockwise) or in both directions if no preference is indicated. The planner then selects as the plan the path with the largest minimum overlap between the angle ranges of adjoining nodes. For

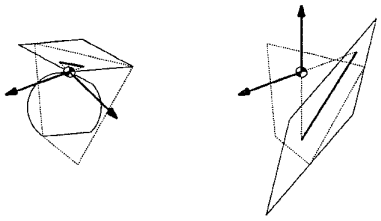

Figure 12: A rotation plan for body $\mathcal{B}$.

each hand-off, the transition angle ψ is taken to be the angle bisector of the overlapping angle range. The transition force focus points $\mathbf{c}_{fik}$ and $\mathbf{c}_{flm}$ are simply the midpoints of the intersections their respective permissible regions with of the line of force corresponding to ψ. The initial and goal force focus points are computed analogously. Receiving and releasing points within a permissible region are connected by a line which denotes the trajectory of $\mathbf{c}_f^{\mathcal{B}}$ within that region. A sequence of graph nodes with transition parameters and trajectories forms a complete plan.

Figure 12 depicts a plan for rotating $\mathcal{B}$ through the orientation range $[\frac{-\pi}{4}, \pi]$. The trajectories of the force focus are drawn as line segments within the permissible regions. Figure 8 shows the commanded contact trajectories derived from this plan and the anticipated motion of the object.

6. Conclusion

In this paper, we have shown how to plan stably supported rotations of convex polygonal objects in the plane of gravity, using two point contacts. In particular, we have derived a mapping from force focus points to local contact configurations at equilibrium, such that each equilibrium configuration corresponds to a unique force focus. For any edge pair, the constraints for geometric contact, force equilibrium and stability project onto the force focus space, giving a simple geometric description of the set of stable support configurations with a contact on each edge. We also show that connectivity in a permissible force focus region implies connectivity in the space of stable support configurations, allowing us to transform force focus trajectories into contact motions which induce rotations of the object. Finally, we have described two rotation planning strategies which use hand-offs between contact pairs, enabling rotations through angles ranges impossible with a single pair of contacts.

References

[1] T. Abell and M. Erdmann. Stably supported rotations of a planar polygon with two frictionless contacts. Technical report, Carnegie Mellon University, to appear.

[2] Z. Balorda. Reducing uncertainty of objects by robot pushing. In *ICRA*, pages 1051–1056, 1990.

[3] D. L. Brock. Enhancing the dexterity of a robot hand using controlled slip. In *ICRA*, pages 249–251, 1988.

[4] R. C. Brost. Computing the possible rest configurations of two interacting polygons. In *ICRA*, pages 686–693, 1991.

[5] M. Erdmann. On a representation of friction in configuration space. *IJRR*, 13(3):240–271, 1994.

[6] R. S. Fearing. Simplified grasping and manipulation with dextrous robot hands. In *Proc. of the Am. Control Conf.*, pages 32–38, 1984.

[7] W. S. Howard and V. Kumar. Stability of planar grasps. In *ICRA*, pages 2822–2827, 1994.

[8] I. Kao and M. R. Cutkosky. Quasistatic manipulation with compliance and sliding. *IJRR*, 11(1):20–40, 1992.

[9] T. Lozano-Pérez. Spatial planning: A configuration space approach. *IEEE Trans. on Computers*, C–32(2):108–120, 1983.

[10] X. Markenscoff, L. Ni, and C. H. Papadimitriou. The geometry of grasping. *IJRR*, 9(1):61–74, 1990.

[11] X. Markenscoff and C. H. Papadimitriou. Optimum grip of a polygon. *IJRR*, 8(2):17–29, 1989.

[12] B. Mishra, J. T. Schwartz, and M. Sharir. On the existence and synthesis of multifinger positive grips. *Algorithmica*, 2(4):541–558, 1987.

[13] D. J. Montana. Contact stability for two-fingered grasps. *IEEE Trans. on R & A*, 8(4), 1992.

[14] V.-D. Nguyen. Constructing force-closure grasps. *IJRR*, 7(3), 1988.

[15] Y. C. Park and G. P. Starr. Grasp synthesis of polygonal objects. In *ICRA*, pages 1574–1580, 1990.

[16] D. Rus. *Fine Motion Planning for Dexterous Manipulation.* PhD thesis, Cornell University, 1992.

[17] J. K. Salisbury and J. J. Craig. Articulated hands: Force control and kinematic issues. *IJRR*, 1(1):4–17, 1982.

[18] J. C. Trinkle. On the stability and instantaneous velocity of grasped frictionless objects. *IEEE Trans. on R & A*, 8(5):560–572, 1992.

[19] J. C. Trinkle, A. O. Farahat, and P. Stiller. First-order stability cells of frictionless rigid body systems. Technical report, Texas A&M University, 1993.

[20] J. C. Trinkle, A. O. Farahat, and P. Stiller. Second-order stability cells of a frictionless rigid body grasped by rigid fingers. In *ICRA*, pages 2815–2821, 1994.

[21] T. Yoshikawa, Y. Yokokohji, and A. Nagayama. Object handling by three-fingered hands using slip motion. In *IROS*, pages 99–105, 1993.